Bubble formation via multidrop impacts

Alexander G. Bick,[1] William D. Ristenpart,[2] Ernst A. van Nierop,[1] and Howard A. Stone[1,a)]
[1]*School of Engineering and Applied Sciences, Harvard University, Cambridge, Massachusetts 02138, USA*
[2]*Department of Chemical Engineering and Materials Science and Department of Food Science and Technology, University of California at Davis, Davis, California 95616, USA*

(Received 28 May 2009; accepted 11 March 2010; published online 29 April 2010)

Gas bubbles are often generated when droplets impact a liquid-air interface. For the impact of single droplets, a critical impact velocity must be exceeded for air to be entrained in the form of bubbles. Here we establish that bubbles can be generated at much lower velocities provided that two or more drops impact the liquid-air interface within a sufficiently short time interval. Using high-speed imaging, we show that bubbles are entrained when a drop lands in the impact crater of a previous drop. We quantify the critical crater depth formed upon impact and the necessary time interval between drop impacts for bubble entrainment to occur. For 1 mm diameter water drops falling at 1 m/s, the critical separation time is approximately 5 ms. This critical time is consistent with a scaling analysis of the time required for an impact crater to close by capillarity. © *2010 American Institute of Physics*. [doi:10.1063/1.3397851]

I. INTRODUCTION

Foams are structures characterized by a large number of gas bubbles trapped within an otherwise continuous solid or liquid phase. Although foams are desirable in a wide range of applications because of their low density, low thermal conductivity, or favorable mechanical properties,[1] there are many situations where foams are the unwanted product of mixing two liquids together. Researchers typically focused on foam behavior *after* it is formed, especially foam rheology[2–4] and drainage dynamics.[5–7] Less is known about foam generation. Previous experimental work focused on foam generation under controlled sparging conditions,[8,9] but foams are often generated under less controlled circumstances, such as when one liquid is poured into another. This ubiquitous process is important for a wide array of industrial applications, and chemical defoaming and antifoaming agents are frequently employed to reduce unwanted foam.[9] A more fundamental understanding of the mechanism of foam formation due to liquid-on-liquid impact will yield insight on ways to minimize foam formation and consequently reduce the use of chemical defoaming agents.

Air entrainment due to the impact of a continuous liquid jet on a liquid-air interface has been studied for several types of jets, including smooth,[10] perturbed,[11] and buckling[12] jets. Often, however, a jet breaks into a stream of discrete drops due to the Rayleigh–Plateau capillary instability. Upon striking the liquid-air interface, these drops can entrain air, which leads to the formation of bubbles. Since foam generation depends on the formation of individual bubbles, examination of bubble entrainment following the impact of individual droplets onto the surface of a liquid bath provides insight on the more complicated foam generation behavior due to a stream of droplets. Early studies of air entrainment following impact of individual drops were motivated by the underwater sound of rain, because the resulting noise is audible to the human ear and is picked up by underwater microphones on ships and submarines.[13,14] Worthington[15] is recognized as the first to investigate the sound made by impacting drops and splashes using high-speed photographic techniques. A key observation was that bubbles are generated by the impact of single droplets only when a critical impact velocity was exceeded, a result corroborated by many subsequent studies.[13,14,16–20]

In this work, we report that bubbles can be generated by impact of drops with sizes and velocities much smaller than those reported previously, provided two drops impact the surface sequentially within a sufficiently short period of time. We refer to this phenomenon as bubble formation via a multidrop impact. We investigate this multidrop entrainment mechanism qualitatively and quantitatively, and rationalize the time lag of the second impacting drop necessary to entrain a bubble from the crater formed by the first drop. The results presented here suggest mechanical, rather than chemical, means to suppress foam formation in processes where liquids are mixed together.

II. EXPERIMENTAL METHODOLOGY AND QUALITATIVE OBSERVATIONS

The experimental apparatus is sketched in Fig. 1(a). A syringe pump pushed a jet ($\mathrm{Re} \sim 10^3$) of distilled water (Millipore) from a nozzle of a given diameter (0.3–1.5 mm). The nozzle was mounted vertically 1–8 cm above a deep bath of distilled water. The jet of water broke up into drops with diameters 0.25–3 mm, which were dependent on the nozzle diameter. By changing the flow rate, impact velocities from 0.5–2 m/s were obtained.

Using a high-speed camera (Photron V9) at frame rates of 3000–9000 frames per second, drops could be observed individually impacting the interface of the air/water

a)Present address: Department of Mechanical and Aeronautical Engineering, Princeton University, Princeton, New Jersey 08544, USA.

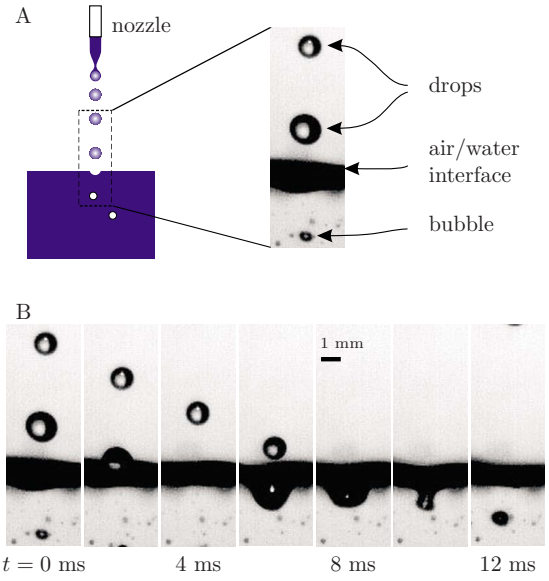

FIG. 1. (Color online) (a) Sketch of the experimental apparatus and representative images of a two-drop impact sequence leading to bubble formation. A jet of distilled water issues from a nozzle and breaks up into drops, and upon impact with the air-liquid interface sometimes resulted in bubble formation. (b) Time sequence of the formation of a single bubble following a multi-(two) drop impact (enhanced online). [URL: http://dx.doi.org/10.1063/1.3397851.1]

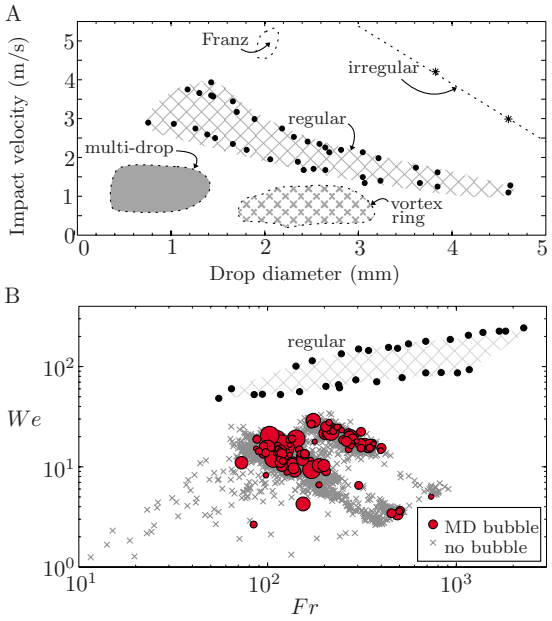

FIG. 2. (Color online) (a) Phase diagram summarizing the different regimes of bubble formation due to the impact of distilled water drops. The "multi-drop" region corresponds to the results reported here; other regimes denote previous observations: Franz (Ref. 14), regular (Ref. 16), vortex ring (Refs. 22 and 23), and irregular (Ref. 16). See text for details. (b) Phase diagram illustrating regular (Ref. 16) and "multidrop" entrainment regions in Froude–Weber number space. The size of the MD bubble markers is proportional to the observed bubble diameters.

bath [Fig. 1(b)]; see video linked to Fig. 1. The deflection of the air-water interface (referred to herein as the crater) was visible in the high-speed images. Qualitatively, the crater forms as a result of the first impacting drop. In the absence of a second impacting drop, the crater simply recovers to its initial flat configuration and no bubble is generated. When a second drop hits the impact crater due to the first drop, however, a bubble can form [Fig. 1(b)]. The objects emitted below the crater were identifiable as bubbles because air has a different index of refraction than the surrounding water; moreover, the objects underwent shape oscillations characteristic of bubble formation[16] and eventually migrated back up toward the air/water interface. Several different reservoir sizes (cross sectional areas 0.5–25 cm^2 and depths 0.1–4 cm) were used to test whether bubble formation was influenced by the concentration of bubbles or by any wall effects. No noticeable difference was observed for the reservoir sizes tested (see Ref. 21 for details). The observations indicate that bubble formation is dominated by the local dynamics of the impact crater and appears insensitive to the presence of any bubbles or walls in the vicinity.

To place our observations in the context of previous work on bubble formation, a phase diagram of known bubble formation behavior due to drop impacts is shown in Fig. 2(a) by reporting the impact velocity versus the drop diameter. There are several different regimes; for single-drop impact, at sufficiently low velocities typically no bubble is produced. If a critical velocity is exceeded, the impact of a single droplet almost invariably produces a bubble with diameter comparable to that of the drop.[16] For a given drop size and velocity the bubble formation is highly reproducible, so this behavior is referred to as "regular" bubble formation. For reasons that are poorly understood, there is a second critical velocity above which bubbles are no longer regularly produced. At very high velocities, bubbles are again generated by the impact of single droplets, but only occasionally and with highly variable size; this regime is referred to as "irregular."[16]

At the smaller velocities studied here, however, the impact of a single drop infrequently results in the formation of many small bubbles (<50 μm) periodically arranged around the impact crater. Since these bubbles are apparently generated by vortices in the fluid, the bubbles are referred to as a "vortex ring."[22,23] From our observations of the formation of several hundred bubbles, two qualitatively different bubble formation events were recognized: the multidrop event and the vortex ring entrainment event. Typically, for every 100 bubble formation events, approximately two were of the vortex ring type. Here we focus on the multidrop mechanism, which under our experimental conditions was by far the most common formation event and is labeled in Fig. 2(a) as "multidrop."

In the multidrop region of parameter space, we emphasize that single droplets fail to generate bubbles. This behavior is explored in more detail in Fig. 2(b), in which our experimental observations of multidrop impacts are compared with the regime of regular bubble entrainment in Froude–Weber number space. Here the Froude number is defined as $\mathrm{Fr} \equiv u^2/gd_{\mathrm{drop}}$ and serves as a comparison of inertial effects to gravitational effects (for a drop of diameter d_{drop} impacting at velocity u), while the Weber number is defined as $\mathrm{We} \equiv \rho u^2 d_{\mathrm{drop}}/\gamma$ and serves as a comparison of inertial effects to surface tension effects (for a liquid with density ρ and interfacial tension γ). Two key points are dem-

onstrated by Fig. 2(b). First, the multidrop bubble formation occurs for comparable Froude numbers as regular entrainment, but at Weber numbers approximately one order of magnitude lower. Second, the multidrop bubble formation is highly irregular, in the sense that not all impacts yield bubbles. Only a small fraction of all impacts (indicated by gray crosses) yielded bubbles (indicated by red circles), an effect explored in more detail in Sec. III.

A literature search did not reveal previous observations of the multidrop phenomenon in the regime of low speeds (<2 m/s) and relatively small drop diameters (d_{drop} <2 mm) investigated here. To our knowledge, the only similar observations were reported by Franz in 1959,[14] who in his investigation of single drop impacts noted that occasionally his equipment malfunctioned and two drops would impact in close succession, generating a bubble. The reported velocities, however, were much higher, ≈ 5 m/s, and are labeled in Fig. 2(a) as "Franz." Our experimental apparatus was unable to generate droplet velocities much above 2 m/s, so an intriguing possibility is that multidrop bubbles form at velocities and sizes much larger than those denoted in Fig. 2, i.e., at higher velocities extending to the region labeled "Franz." Further experiments will be necessary to test this hypothesis; here we focus on lower velocities to illustrate and explain the basic phenomenon.

To test whether the multidrop mechanism is specific to de-ionized water or occurs more generally, our apparatus was also used to examine liquids with surfactants present (e.g., 2% sodium dodecyl sulfate) as well as carbonated beverages (e.g., beer). In each case bubbles were observed to form via a multidrop impact (see video at Ref. 21). These qualitative observations confirm that the underlying phenomenon—bubble formation via multidrop impacts—is reproducible in liquid systems other than de-ionized water. All of the following quantitative measurements were obtained with de-ionized water without additional surfactants; these measurements will serve as a basis of comparison for future experiments with more complicated systems.

III. QUANTITATIVE RESULTS AND DISCUSSION

Quantitative data about the drop impacts and resulting bubble formation were obtained from the high-speed videos using custom image analysis routines in MATLAB (see Appendix for details). The size and position of every drop and bubble, as well as the current depth of the impact crater, were extracted from each frame in the video. Linear fits of the position versus time were used to determine the drop impact velocities.

A typical data set is shown in Fig. 3. The diameter and time of impact of every drop during a 50 ms period is plotted, as well as the resulting crater depth and bubble diameters. Note that the crater depth (indicated by the solid line) invariably increases shortly after a drop impact (denoted by the triangles), but that only a small fraction of impacts was followed by bubble formation (denoted by the circles). In the course of ten separate 1 s long trials using the same flow rate and nozzle diameter, only 139 bubbles were produced by a

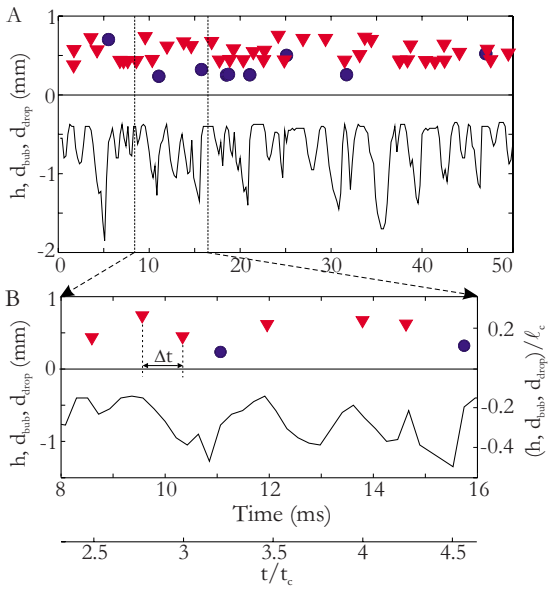

FIG. 3. (Color online) (a) Representative data for the dynamics of bubble formation due to multidrop impacts. Symbols are as follows: (▼) the drop diameter d_{drop} at the time of impact, (●) the bubble diameter d_{bub} immediately after separation from the crater, and (solid line) the crater depth h. For clarity the crater depth is offset from zero by 0.2 mm. (b) Magnification of the same data set as in (a) showing two pairs of drop impacts that result in bubble formation.

multidrop mechanism out of approximately 2000 drop impacts. This observation suggests that the bubble formation process is at least partially stochastic.

The occurrence of bubbles in Fig. 3 may appear random, but analysis of the complete data set reveals several underlying correlations. First, in accord with the qualitative observations, it is clear that bubbles only form when the crater depth h exceeds a critical value (Fig. 4). The distribution of maximal crater depths following every drop impact differs dramatically from the distribution of crater depths immediately preceding bubble formation [Fig. 4(a)]. Whereas the mean crater depth for all impacts was 1.02 mm with standard deviation 0.96 mm, the distinct subset of bubble-generating craters had a mean crater depth of 2.52 mm with standard deviation of 0.89 mm; essentially no bubbles were formed for $h<1.25$ mm. Less than 5% of all observed craters met this minimum depth criterion. A key point is that the critical crater depth is approximately equal to the capillary length, $\ell_c=\sqrt{\gamma/\rho g}\approx 2$ mm; essentially no bubbles formed if $h/\ell_c \ll 1$.

Since multidrop impacts only generated bubbles in sufficiently deep craters, it is natural to ask whether the bubble size increases with crater depth (since there is a larger volume of air to entrain). A plot of the bubble diameter d_{drop} versus the preceding crater depth, however, shows no clear trend [inset, Fig. 4(b)]. The minimal crater depth is clearly observed, but no other clear correlation between d_{drop} and h is observed. Because the drops were formed via the Rayleigh–Plateau instability, the drop sizes are not uniform and one possible explanation for the lack of a clear trend between d_{drop} and h is that only sufficiently large drops generated bubbles upon impact. The data in Fig. 5 indicate, how-

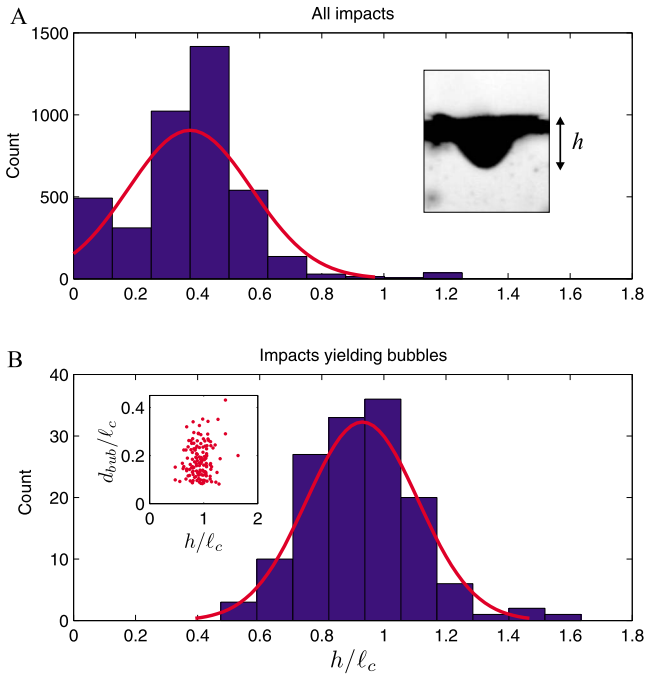

FIG. 4. (Color online) (a) Histogram of the observed maximal crater depth h following every drop impact and (b) for those immediately preceding bubble formation, with distances scaled on the capillary length ℓ_c. Note that the drops were falling onto a dynamic surface, so the crater depth depended in general on the size and timing of preceding drops. Solid lines show best fits to a normal distribution. Inset shows plot of bubble diameter vs the preceding maximal crater depth; no clear correlation is observed. Note that our image analysis procedure precluded measurement of bubbles smaller than approximately 0.2 mm because they were difficult to differentiate from noise.

ever, that the diameters of both the first and second drops immediately prior to each bubble generation event are representative of the overall distribution of falling drops. Taken together, the data in Figs. 4 and 5 suggest that the mechanism behind bubble entrainment is more complicated than merely capturing all of the air in the crater into a bubble.

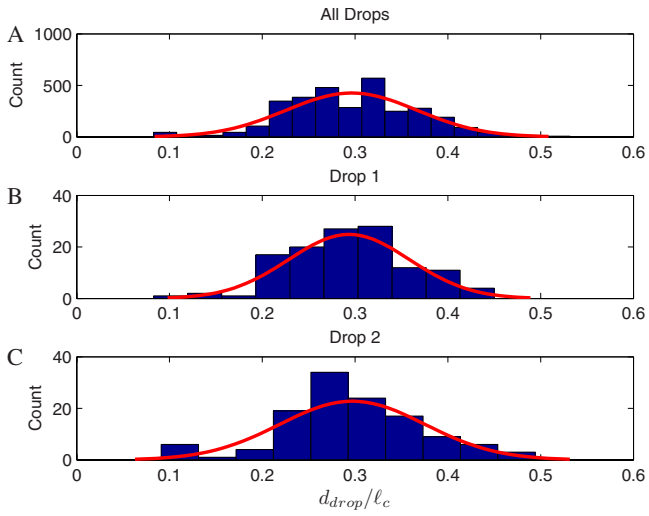

FIG. 5. (Color online) Histograms of drop diameter in millimeters for (a) all drops, (b) first impacting drop, and (c) second impacting drop. The size distribution of drops which formed bubbles is similar to the overall distribution of all impacting drops.

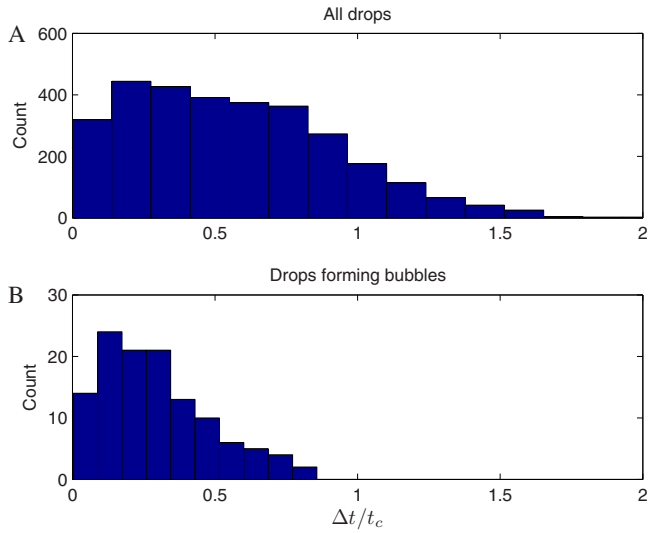

FIG. 6. (Color online) Histograms of Δt for each pair of multidrop impacts which (a) did not form a bubble (b) formed a bubble. Note the critical time interval $\Delta t = 5$ ms ($\Delta t/t_c \approx 0.8$) above which no bubbles formed.

Although differences in drop size do not appear to affect the probability of bubble generation, the data indicate that the time interval Δt between drop impacts is crucial. The distributions of Δt for all droplet pairs and the droplet pairs that immediately preceded bubble formation are shown in Fig. 6. We observe that the bubble-generating drop pairs represent a distinct subset defined by the critical time interval $\Delta t \leq 5$ ms. Thus, generation of a sufficiently deep crater by the first impacting drop is insufficient to generate a bubble; a second drop must also land inside the crater within a sufficiently short time period.

The magnitude of the critical time interval can be understood in terms of the time required for a crater to recover back to a flat configuration by capillarity. Note that the length scales of interest here are comparable with or smaller than the capillary length ℓ_c. Moreover, at impact the drop Weber number is of the order of 10 and the Froude number is of the order of 10^2 to 10^3, so it is plausible that a balance of capillary forces and inertia governs the crater dynamics. Accordingly, the time required for a crater of depth h to close up by capillarity is approximately

$$t_c \sim \left(\frac{\rho h^3}{\gamma}\right)^{1/2}. \tag{1}$$

For values typical of our experiments $t_c \approx 5-20$ ms, consistent with the observed critical time interval. Thus, if $\Delta t/t_c > 1$, then the crater created by the impact of the first drop fills in to an extent such that bubble formation is no longer possible. Note that the exact details of the crater collapse are possibly affected by gravitational effects, since $h \approx \ell_c$ and the Bond number $\rho g h^2/\gamma$ is of the order of 1. The predicted time scale for gravitational effects is slightly larger at $\tau_g = \sqrt{h/g} \approx 40$ ms. The key point is that for either case the time scale for the dynamics of the collapse is estimated to be of the order of 5–40 ms; no bubbles were generated for values of Δt that exceeded this value.

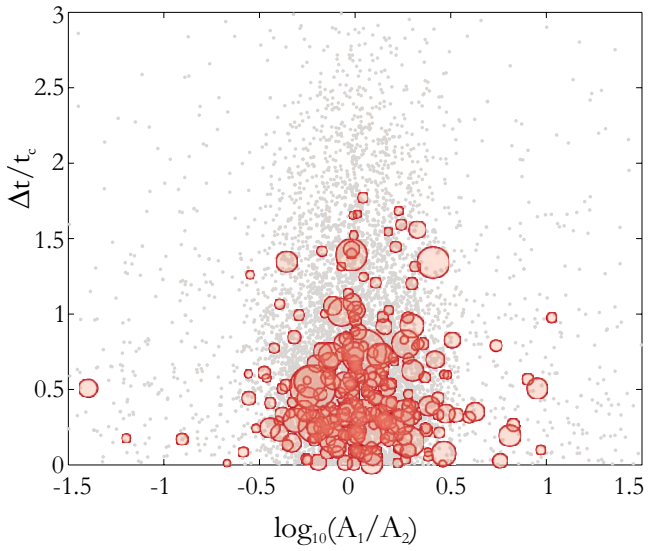

FIG. 7. (Color online) A plot of the ratio of drop sizes against the corresponding time interval between the two drops. The dots indicate drop pairs that do not form bubbles while the circles indicate that a bubble was formed. The diameter of each circle is scaled with the measured bubble diameter to give an indication of the size distribution of bubbles. The "drop area ratio," A_1/A_2, is plotted on a log scale so as to center the drops of equal sizes at 0. It appears that there is no difference in bubble production if the first drop is bigger or smaller than the second drop. The critical time threshold of approximately 5 ms for bubble formation can be observed as well. The stochastic nature of multidrop entrainment is highlighted by the numerous impacts below the critical time which do not form bubbles.

Because the time interval plays a key role, we examined the possibility that the order of impacting drop sizes is significant—in other words, bubbles might form only when a large drop lands in a comparatively narrow crater formed by a smaller drop, thereby trapping the air and forming a bubble. To test this hypothesis, we examined the effect of the drop diameters $d_{\mathrm{drop},1}$ and $d_{\mathrm{drop},2}$; here the subscript 1 denotes the first drop that hits the surface and 2 denotes the following drop. The time interval Δt is plotted versus the "drop area ratio" $A_1/A_2=d^2_{\mathrm{drop},1}/d^2_{\mathrm{drop},2}$ in Fig. 7, where we distinguish all of the impacts (dots) from those events that actually yielded bubbles (shaded circles). The distribution of bubble generation events indicates that bubble formation is insensitive to the order of drop impact. Bubbles are equally likely to form regardless of whether the first drop is smaller, larger, or the same size as the second drop (the left and right sides of Fig. 7, respectively). Moreover, it does not appear that a small drop followed by a large drop or vice versa necessarily creates a larger or smaller bubble. Histograms of bubble diameter (see supplementary material) show that there is no significant difference in the total number of resulting bubbles or their size with respect to the drop order.

Finally, we tested whether the shape of the drops or deviations in their impact location played any role in bubble formation. Because the drops are formed by the breakup of a continuous jet via the Rayleigh–Plateau instability, they tend to oscillate as they fall,[24] alternating between prolate and oblate orientations. Although the final drop shape prior to impact was not observable, we were able to examine the final observable shape (prior to entry into the crater). The shape was parametrized by the eccentricity, i.e., the scalar between 0 and 1 that characterizes the shape of the ellipse that has the same second moments as the object. No noticeable difference in bubble generation probability was observed for drops with large or small eccentricities (see supplementary material), suggesting that the bubble formation is not highly sensitive to the exact shape of the impacting drop. Likewise, it is possible that horizontal deviations in the impact location play a role in the bubble formation (i.e., if the second drop lands off-center in the crater). Histograms of the bubble generation probability versus observed lateral deviation revealed no significant effect. However, our experimental setup is limited in that we can only view in one direction at a time, so it is possible that we miss deviations in the direction parallel to the viewing direction (i.e., oriented out of the page in Fig. 1). Further experimentation, ideally with two cameras set up orthogonally to capture the full three-dimensional trajectories, will be necessary to test these possibilities in more detail.

IV. CONCLUSIONS

In this paper we report that multidrop impacts cause bubble entrainment in a velocity and drop size regime in which single drop impacts fail to generate bubbles. In making these observations we expand on a comment apparently first made by Franz[14] who noted that occasionally a second small drop following a first large drop will result in a small bubble being produced; however, we observe multidrop bubble formation at significantly smaller velocities than Franz. Moreover, our quantitative measurements revealed three key characteristics of multidrop impacts. (1) Bubbles only form when a critical crater depth is exceeded. (2) Bubbles do not form if a critical time interval following the preceding drop impact is exceeded. (3) Bubble formation and size are insensitive to the size and order of the preceding drop pair. Additional theoretical work is necessary to clarify the mechanism underlying multidrop bubble entrainment, and further experimental work is necessary to establish if multidrop bubble formation occurs at other drop velocities and sizes.

Although the details of the bubble formation mechanism are not yet clear, an important practical implication of our observations is that a purely mechanical method may suppress foam formation without the use of chemical antifoaming agents. Specifically, the existence of a critical time interval suggests that bubble formation can be reduced by any process that prevents two drops from impacting the same location within the critical time interval. For example, bubble generation will be prevented if the liquid-dispensing nozzle described in our experimental setup is mounted on a spinning disk that moves with an angular velocity sufficiently large to prevent two drops from impacting in the same location within the critical time interval. We will report such a device in a future communication.

ACKNOWLEDGMENTS

We thank the Harvard Nanoscale Science and Engineering Center for partial funding, and we thank C. Bamforth for inspiring our examination of foam formation in beer.

APPENDIX: IMAGE ANALYSIS

Images from the high-speed videos were analyzed using custom-written programs in MATLAB. The gray scale images were first converted to binary via thresholding. Detected objects smaller than 25 pixels in area (primarily noise) were removed. Bubbles were identified within a region just below that of the minimum value of the crater. When the crater depth was observed to change rapidly [as in Fig. 3(b), middle trace around 11 and 15–16 ms], the bubble-tracking code was triggered to look for the closest circular object to the last known location of the crater minimum. Any bubble that was found was tracked for five frames and the average bubble size, shape, and position were recorded. To ensure the accuracy of the computer analysis, each movie was manually reviewed and each bubble individually confirmed to be an actual bubble and not an artifact of the image processing. Any bubbles that were not identified by the computer could also be manually selected and tracked. The accuracy of the image analysis depended on the quality of the video, including noise in each frame, and ranged from 0%–10% false positive identification of bubbles and 0%–3% bubbles missed in a given movie; these errors were corrected by the manual check. The uncertainty in our edge detection analysis is approximately 1 pixel. For typical magnifications in our setup, the calibration was approximately 250 pixels/mm, yielding an error of ± 4 μm which is small compared to the typical drop length scale of ≈ 1 mm.

[1] D. L. Weaire and S. Hutzler, *The Physics of Foams* (Oxford University Press, New York, 1999).
[2] H. M. Princen, "Rheology of foams and highly concentrated emulsions. 1. Elastic properties and yield stress of a cylindrical model system," J. Colloid Interface Sci. **91**, 160 (1983).
[3] S. A. Khan and R. C. Armstrong, "Rheology of foams. 1. Theory for dry foams," J. Non-Newtonian Fluid Mech. **22**, 1 (1986).
[4] D. J. Durian, "Foam mechanics at the bubble scale," Phys. Rev. Lett. **75**, 4780 (1995).
[5] G. Verbist, D. Weaire, and A. M. Kraynik, "The foam drainage equation," J. Phys.: Condens. Matter **8**, 3715 (1996).
[6] S. A. Koehler, S. Hilgenfeldt, and H. A. Stone, "Liquid flow through aqueous foams: The node-dominated foam drainage equation," Phys. Rev. Lett. **82**, 4232 (1999).
[7] H. A. Stone, S. A. Koehler, S. Hilgenfeldt, and M. Durand, "Perspectives on foam drainage and the influence of interfacial rheology," J. Phys.: Condens. Matter **15**, S283 (2003).
[8] L. G. Phillips, Z. Haque, and J. E. Kinsella, "A method for the measurement of foam formation and stability," J. Food Sci. **52**, 1074 (1987).
[9] R. J. Pugh, "Foaming, foam films, antifoaming and defoaming," Adv. Colloid Interface Sci. **64**, 67 (1996).
[10] E. Lorenceau, D. Quere, and J. Eggers, "Air entrainment by a viscous jet plunging into a bath," Phys. Rev. Lett. **93**, 254501 (2004).
[11] Y. G. Zhu, H. N. Oguz, and A. Prosperetti, "On the mechanism of air entrainment by liquid jets at a free surface," J. Fluid Mech. **404**, 151 (2000).
[12] B. Pouligny and M. Chassande-Mottin, "Air ingestion by a buckled viscous jet of silicone oil impacting the free surface of the same liquid," Phys. Rev. Lett. **100**, 154501 (2008).
[13] E. G. Richardson, "The sounds of impact of a solid on a liquid surface," Proc. Phys. Soc. London, Sect. B **68**, 541 (1955).
[14] G. J. Franz, "Splashes as sources of sound in liquids," J. Acoust. Soc. Am. **31**, 1080 (1959).
[15] A. M. Worthington, *A Study of Splashes* (Longmans, London, 1908).
[16] H. C. Pumphrey, L. A. Crum, and L. Bjorno, "Underwater sound produced by individual drop impacts and rainfall," J. Acoust. Soc. Am. **85**, 1518 (1989).
[17] A. Prosperetti, L. A. Crum, and H. C. Pumphrey, "The underwater noise of rain," J. Geophys. Res., [Oceans] **94**, 3255, doi:10.1029/JC094iC03p03255 (1989).
[18] H. N. Oguz and A. Prosperetti, "Bubble entrainment by the impact of drops on liquid surfaces," J. Fluid Mech. **219**, 143 (1990).
[19] H. Medwin, J. A. Nystuen, P. W. Jacobus, L. H. Ostwald, and D. E. Snyder, "The anatomy of underwater rain noise," J. Acoust. Soc. Am. **92**, 1613 (1992).
[20] A. Prosperetti and H. N. Oguz, "The impact of drops on liquid surfaces and the underwater noise of rain," Annu. Rev. Fluid Mech. **25**, 577 (1993).
[21] See supplementary material at http://dx.doi.org/10.1063/1.3397851 for high speed videos and additional statistical analyses.
[22] K. Carroll and R. Mesler, "Bubble nucleation studies. 2. Bubble entrainment by drop-formed vortex rings," AIChE J. **27**, 853 (1981).
[23] F. Rodriguez and R. Mesler, "The penetration of drop-formed vortex rings into pools of liquid," J. Colloid Interface Sci. **121**, 121 (1988).
[24] E. F. Goedde and M. C. Yuen, "Experiments on liquid jet instability," J. Fluid Mech. **40**, 495 (1970).